Model-based feedforward control for an optimized manipulation of acoustically levitated spheres

Marco A. B. Andrade, Sebastian Zehnter, Felix Funke, Christoph Ament

Model-based feedforward control for an optimized manipulation of acoustically levitated spheres

Marco A. B. Andrade ✉ ; Sebastian Zehnter ✉ ; Felix Funke ✉ ; Christoph Ament ✉

Check for updates

View Online   Export Citation

Model-based feedforward control for an optimized manipulation of acoustically levitated spheres

View Online   Export Citation   CrossMark

Marco A. B. Andrade,[1,a] ID **Sebastian Zehnter,**[2,a] ID **Felix Funke,**[2,a] ID **and Christoph Ament**[2,a] ID

AFFILIATIONS

[1] Institute of Physics, University of São Paulo, São Paulo 05508-090, Brazil
[2] Chair of Control Engineering, University of Augsburg, Augsburg 86159, Germany

[a] Authors to whom correspondence should be addressed: marcobrizzotti@gmail.com; sebastian.zehnter@uni-a.de; felix.funke@uni-a.de; and christoph.ament@uni-a.de

ABSTRACT

We present a simple dynamic model for predicting the manipulation behavior of an acoustically levitated sphere. The model allows for the calculation of the sphere position over time, which is demonstrated for two manipulation strategies: a straight motion with a constant manipulation velocity and a straight motion in which the sphere acceleration follows a cosine function. The dynamic model as well as the manipulation strategies is verified experimentally in an acoustic levitator system consisting of an array of 16 by 16 ultrasonic transducers emitting at 40 kHz and an opposing reflector. In this system, a glass sphere of a diameter of 2 mm is manipulated horizontally by controlling the phases of the transducers. The sphere motion is recorded using a high-speed camera, and a tracking algorithm is used for capturing the sphere position over time. Moreover, a model predictive control algorithm is applied on a path-following problem to move the sphere along a given reference trajectory by means of a model-based optimal feedforward control. The proposed dynamic model as well as the methodology presented in this paper enables faster manipulation speeds with reduced oscillations during object movement.

I. INTRODUCTION

Acoustic levitation[1] relies on the phenomenon of acoustic radiation force[2] to suspend and manipulate small objects in mid-air. Due to its versatility to suspend liquid[3,4] or solid[5,6] objects, acoustic levitation is a promising technique for numerous disciplines, such as chemistry,[7] biology,[8] pharmacy,[9,10] and industry.[11]

Among different acoustic levitation strategies,[6,12–15] the most common approach uses standing wave fields such that an object smaller than half of the acoustic wavelength is trapped at a pressure node of the standing wave.[16,17] This approach allows not only the suspension of the object but also its manipulation by changing the position of the pressure node. This can be done by either adjusting the voltage amplitude,[18] relative phase,[19–21] or frequency[22] of the transducers.

For a long time, acoustic levitation relied on high-power Langevin transducers,[21,23–25] but in 2014, Ochiai, Hoshi, and Rekimoto[20,26] presented a levitation system based on arrays of low-power ultrasound transducers operating at 40 kHz. The use of phased arrays opened up many possibilities in acoustic levitation, such as the manipulation of levitated objects in two[27,28] and three[26] dimensions, use of holographic algorithms for controlling the trapping position,[29] independent manipulation of multiple particles,[30] and contactless assembly of objects,[31] among other possibilities.[32–36]

Despite the recent advances in the contactless manipulation of small objects by acoustic levitation methods, the particles show undesired oscillations,[37,38] even at low speeds, hindering the usage of acoustic levitation in industrial applications. To overcome these limitations, it is of fundamental importance to develop a dynamic model to predict the position of the object over time. Such a model

allows the creation of new strategies that can increase the manipulation speed and reduce undesired oscillations when moving levitated objects.

In this paper, we present a simple dynamic model for manipulating small acoustically levitated spheres. The model is used for calculating the sphere position over time for different acoustic manipulation strategies. We also apply a model predictive control (MPC) algorithm on a path-following problem to optimize the motion of the levitated object. The results predicted by the model are verified experimentally by manipulating a levitated glass sphere and capturing its position over time with a high-speed camera.

II. EXPERIMENTAL SETUP

To investigate the manipulation dynamics, a glass sphere of a diameter of 2 mm and a density of 2540 kg/m^3 is suspended and manipulated horizontally by an acoustic standing wave field that is generated between a plane reflector and an array of ultrasonic transducers emitting acoustic waves at a frequency of 40 kHz (Fig. 1). The phased array contains 256 circular transducers (Manorshi MSO-P1040H07T) of a diameter of 9.8 mm, which are arranged in a square grid of 16 by 16 transducers, with a 10.5 mm spacing between two adjacent transducers. The emission phase of each transducer is programmed in our control software with a phase resolution of $\pi/16$ rad and sent to the array via a serial port (baud rate of 250 kbit/s). Further details of the phased array are described in Ref. 39. For all the measurements, the transducers are electrically excited with a square wave signal of 12 V$_{\text{peak-to-peak}}$ centered at 6V, but they emit sinusoidal waves due to their narrow bandwidth.[40]

The reflector surface lies over the xy plane at $z = 0$, and the phased array is located over the xy plane at $z = 110$ mm. This separation distance between the array and the reflector was chosen because it provides maximum amplitude when the array is focusing at the reflector.[28] As described in previous studies,[27,28] a localized standing wave can be generated above a focal point located over the reflector plane. In this case, the reflector acts as a virtual array located at $z = -110$ mm, which emits the same phases as the phased array (see Fig. S1 in the supplementary material). Consequently, manipulation of the levitated object along the z direction is not possible when using this simple focusing technique because the phases from the phased array and the phases of the virtual array would be offset, defocusing the generated focal point. Since the sphere is suspended at a trapping point located above the focal point, the sphere can be
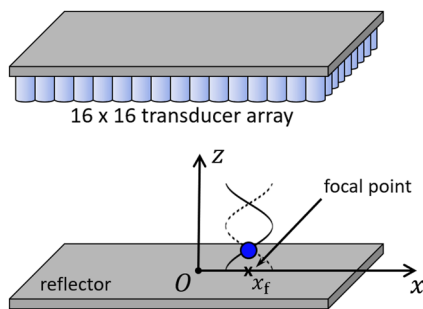
manipulated horizontally by moving the position of the focal point over the xy plane. In this study, the focal point position is denoted by (x_f, y_f, z_f). The manipulation was solely performed along the x direction but can analogously be performed along the y direction due to the symmetry of the experimental setup. The focal point position is controlled by changing the phase of each transducer at a switching rate of 10.32 ms. This switching rate is limited by the transfer of the new phases to the FPGA requiring 2580 bits for a full set of phases and commands for setting the phases. In all the experiments, the glass sphere is trapped at the bottom pressure node of the standing wave, at a height of $z \approx \lambda/4$ above the reflector, where λ is the acoustic wavelength.

The sphere motion is recorded using a high-speed camera (Photron FASTCAM MINI UX50) at 500 fps, with a spatial resolution of 26.48 pixels/mm. A tracking algorithm implemented in MATLAB is used to obtain the position of the sphere over time.

III. DYNAMIC MODEL

In this section, we present a simplified dynamic model for predicting the sphere motion along the x direction. In this direction, we assume that only two forces act on the sphere: the acoustic radiation force and the drag force. Therefore, using Newton's second law, the equation of motion for the sphere can be written as

$$m\frac{d^2x}{dt^2} = F_{\text{rad}} + F_{\text{drag}}, \qquad (1)$$

where m is the sphere mass, F_{rad} is the acoustic radiation force, and F_{drag} is the drag force. For small displacements of the sphere with respect to the trapping point, F_{rad} can be approximated by Hooke's law.[41,42] For our experimental setup, this approximation has an error of less than 1% for displacements of less than ±0.5 mm and less than 5% for sphere displacements of up to ±1 mm (see Fig. S4 in the supplementary material). In our model, we assume that the trapping position is located at a height of $z \approx \lambda/4$ above the focal point position x_f. Therefore, the acoustic radiation force F_{rad} along the x direction can be described by

$$F_{\text{rad}} = -\kappa(x - x_f), \qquad (2)$$

where κ is the stiffness constant and x is the horizontal position of the sphere. For the drag force F_{drag}, we assume a linear model with a damping coefficient b that is calculated as

$$F_{\text{drag}} = -b\frac{dx}{dt}. \qquad (3)$$

Given the sphere initial position x_0, the initial sphere velocity v_0, the focal point trajectory $x_f(t)$, and the model parameters m, κ, and b, the sphere horizontal position over time $x(t)$ is calculated by solving Eq. (1) numerically. Here, we employ a simple Euler algorithm for solving Eq. (1), with a time step of 1 μs.

The dynamic model is used for calculating $x(t)$ for two distinct manipulation strategies, namely, a linear and a cosine motion. For both cases, $x_f(t)$ is altered at a switching rate of 10.32 ms. For the linear motion, $x_f(t)$ increases linearly from the start position x_{start}

FIG. 1. Illustration of the experimental setup.

to the final position x_{end}. For the cosine motion, $x_f(t)$ is altered according to

$$x_f(t) = \frac{(x_{start} + x_{end})}{2} + \frac{(x_{start} - x_{end})}{2} \cos(\theta), \qquad (4)$$

where the variable θ varies from 0 at x_{start} to π at x_{end}, which results in $\theta = \pi t / t_{end}$.

IV. CHARACTERIZATION OF THE ACOUSTIC TRAP AND EXPERIMENTAL DETERMINATION OF MODEL PARAMETERS

The simplified dynamic model described by Eq. (1) does not consider external disturbances and other random forces acting on the levitated sphere. Therefore, according to the model, if the sphere is displaced from its equilibrium position and then released, the sphere would oscillate around the trapping position until the drag force would damp the oscillatory motion. However, it is well known that a levitated sphere presents small oscillations[37,38] caused by acoustic streaming.[43–45] To characterize the oscillatory behavior of the sphere, the focal point was set to $x_f = 0$ and the glass sphere was suspended at the first pressure node located above the focal point, at a height of $z \approx \lambda/4$.

The sphere's oscillatory behavior was captured using the high-speed camera recording at 500 fps. The sphere's horizontal and vertical positions over time are shown in Figs. 2(a) and 2(c), respectively. The corresponding Fast Fourier Transforms (FFTs) of these signals are presented in Figs. 2(b) and 2(d). As shown in Fig. 2, the sphere presents an oscillatory motion with a random horizontal displacement that can vary from $x = -0.3$ mm to $x = +0.3$ mm. In comparison with the horizontal displacement, the displacement in z was significantly lower, with a maximum displacement that varied from less than ± 0.03 mm with respect to the equilibrium position of the sphere at $z_{eq} \approx 2.10$ mm. This vertical equilibrium position is close to the position of the first pressure node located at a distance of $z \approx \lambda/4$ from the reflector surface. Regarding the FFT, the oscillation in x presents a peak at 8.13 Hz, and the oscillation in z has a peak at 30.82 Hz. These peaks are associated with the corresponding trapping stiffnesses in x and z directions. Since the stiffness scales with the resonance frequency squared, the trapping stiffness along the z direction is ~14.4 times higher than the trapping stiffness in x. In addition to the main peaks, we can also observe in Figs. 2(b) and 2(d) that the sphere presents a low-frequency oscillation between 0 and 3 Hz. The oscillation in this frequency range seems to be caused by time-varying forces due to an unsteady acoustic streaming.[43,44]

After characterizing the oscillatory behavior of the sphere for a fixed value of the focal point ($x_f = 0$), the model parameters
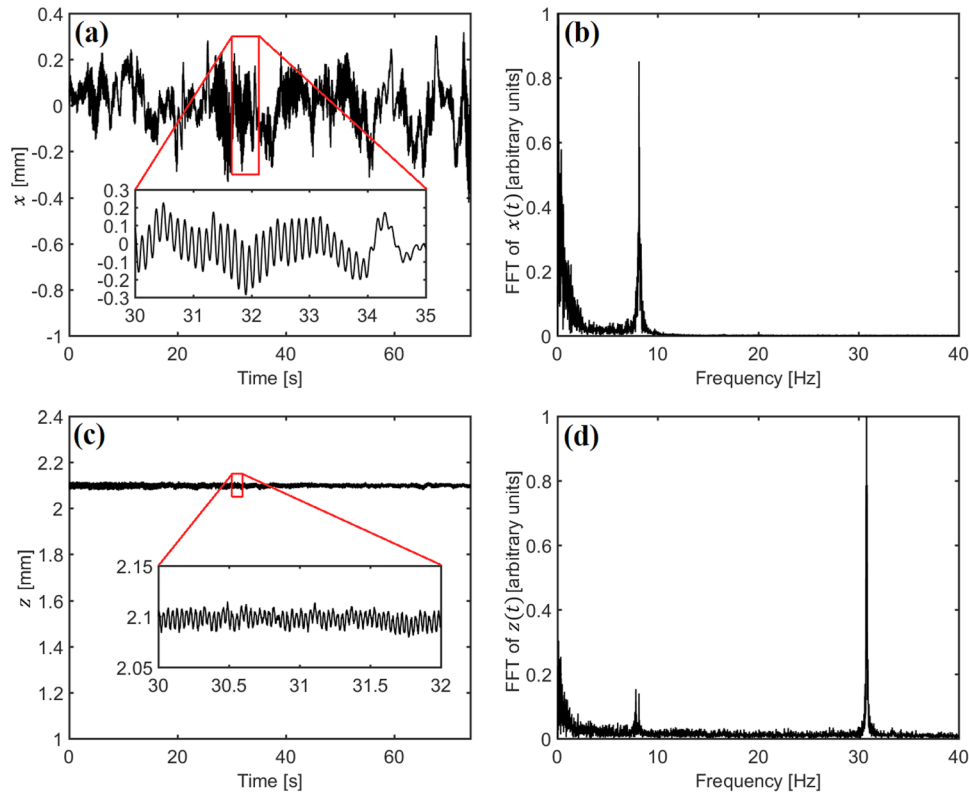
FIG. 2. Sphere position over time along the x and z directions and its corresponding FFT: (a) sphere position in the x direction; (b) FFT of x(t); (c) sphere position in the z direction; (d) FFT of z(t).

17 May 2024 14:15:04

FIG. 3. Damped oscillatory motion of the sphere after switching the focal point position from $x_f = 1$ mm to $x_f = 0$ mm. The experimental curve (in red) was filtered by a low-pass Butterworth filter, and the black curve was fitted to the experimental curve to find the trapping stiffness κ and the damping coefficient b.

were identified from the experiment. The sphere mass $m = 10.64$ mg was calculated based on its radius $a = 1$ mm and its density $\rho = 2540$ kg/m^3. The trapping stiffness κ and the damping coefficient b were obtained by recording the damped oscillatory motion of the sphere after switching the focal point position from $x_f = 1$ mm to $x_f = 0$ mm. After capturing the horizontal position of the sphere over time with the high-speed camera, a fourth-order Butterworth high-pass filter with a cut-off frequency of 5 Hz was applied to the sphere position $x(t)$ to reduce the low-frequency oscillation in the 0–3 Hz frequency range. The filtered sphere position over time was then identified by a damped oscillatory curve to determine the trapping stiffness and the damping coefficient. This procedure resulted in a trapping stiffness $\kappa = 27.4 \times 10^{-3}$ N/m and a damping coefficient $b = 4.35 \times 10^{-6}$ Ns/m. The comparison between the experimental filtered curve and the simulated curve is shown in Fig. 3.

V. TRAJECTORY PLANNING BY MODEL PREDICTIVE CONTROL

To move an object from a position $r_0 \in \mathbb{R}^{3 \times 1}$ smoothly along a discretized trajectory $T = \{r_0, r_1, r_2, \cdots, r_l\}$, it is necessary to determine a sequence of activations $A = \{\phi_0, \phi_1, \phi_2, \cdots, \phi_l\}$ for the phased array. Since our phased array[39] consisting of $N = 256$ transducers only allows phase modulation, our goal is therefore to determine a feasible set A of phase angle vectors $\phi \in \mathbb{R}^{N \times 1}$. Although phase modulation is probably the most widely used method of controlling the transducers of a phased array, it is noteworthy that the simultaneous modulation of amplitude and phase[46] as well as an additional frequency modulation[47] has also been used successfully in the past, opening up the possibility of creating more complex sound fields. While there are several methods[33,48–51] to calculate the acoustic radiation force $F_{rad}(r, \phi) \in \mathbb{R}^{3 \times 1}$ exerted by an array of transducers on an object placed at r for a given ϕ, the inverse projection $F_{rad}^{-1}(r)$ is ambiguous since a feasible ϕ usually cannot be inferred directly from a desired force $F_{rad}(r)$. This circumstance is caused by the strongly correlated nonlinear dependencies between ϕ and F_{rad} and is one of the major problems that currently persist when using acoustic levitation for the dynamic manipulation of

objects. To overcome this issue, two main approaches have been proposed in the literature so far. One option is to obtain every $\phi_i \in A$ by formulating separate optimization problems and solve all of them *a priori* by employing optimization-based methods.[33,50,51] Although this approach can be applied to different object geometries and sizes, its computational costs are very high as time-consuming force models are usually utilized, basically limiting this approach to offline applications as feedforward control. Another option is the usage of holographic acoustic elements.[29] Starting from a feasible activation ϕ_0 that stably suspends an object at r_0, the vector ϕ_0 is split up into a focal lens $\phi_{f,0}$ and a trap signature $\phi_{trap,0} = \phi_0 - \phi_{f,0}$, where the components $\phi_{f,0,j}$ of $\phi_{f,0}$, $j \in 1, 2, \cdots, N$, are given by

$$\phi_{f,0,j} = -k \| r_0 - r_{t,j} \|_2, \tag{5}$$

where k is the wave number and $\| r_0 - r_{t,j} \|_2$ is the Euclidean distance between r_0 and the position $r_{t,j} \in \mathbb{R}^{3 \times 1}$ of the j-th transducer of the phased array. To calculate a feasible activation $\phi_i \in A$ for a corresponding position $r_i \in T$, one can use the approximation

$$\phi_{i,j} \approx \phi_{trap,0,j} + \phi_{f,i,j} \tag{6}$$

for the components $\phi_{i,j}$ of ϕ_i, $j \in 1, 2, \cdots, N$, to refocus the sound pressure field of the acoustic trap from r_0 to $r_i \in T$. Since the computational costs are minimal, the real-time capability of this approach is ensured. Therefore, this method is a frequently used technique to move levitated objects by means of a pure kinematic open-loop control. Here, the movement of an object from r_0 to r_n is simply realized by consecutive refocusing of the acoustic trap at positions $r_i \in T$ at specific times t_i, ensuring a sufficiently small step size $s = \| r_{i+1} - r_i \|_2$, e.g., $s \leq 0.2$ mm, between two adjacent positions r_i and r_{i+1} in each step to prevent the object from being ejected out of the trap.[52] Although this algorithm appeals with its simplicity, there are two major drawbacks that have not yet been resolved. First, looking at the widely used piston source model [see Eq. (7) in the work by Marzo *et al.*[29]], it becomes clear that this method only approximates the phase of the resulting complex pressure but does not take changes in its amplitude into account. These changes in amplitude are caused by the geometric refocusing from the initial location of the trap to adjacent positions. Thus, the approach yields only accurate results in a small working space $W = \{r_{trap,i} \in \mathbb{R}^3 \| \| r_{trap,i} - r_{trap,0} \|_2 \leq \varepsilon\}$ centered around the initial position $r_{trap,0}$ of the trap, where $\varepsilon \in \mathbb{R}^+$ is usually in the range of a few millimeters. If the distance ε between $r_{trap,0}$ and $r_{trap,i}$ is too big, the movement of the trap to $r_{trap,i}$ will cause a strong mismatch of the radiation force distribution. This will lead to a large deviation of the new equilibrium position of the object from the new center of the trap or to an unstable trap. Second, no dynamic model is included in the algorithm. Thus, the object can only be accurately moved at low speeds in a quasi-static behavior when its inertia is not of importance. To overcome the latter issue, we propose the usage of a model-based optimal feedforward control to precisely move a levitated object along the main axis of the acoustic trap, which is the horizontal axis in our application. Although this is a major restriction to the general case, it has only minor implications to our experimental setup (see Fig. 1) and the corresponding numerous applications that are linked with standing wave acoustic levitation, for example, the contactless mixing of droplets.[28] In contrast, this restriction has two

significant advantages. First, it ensures that our assumption of a spring-based model is valid, which is used to predict the radiation force exerted on an object after a small displacement of the acoustic trap [see also Eq. (2) and Fig. 5 in the recent work by Jiang *et al.*].[53] Second, although the feasible region of displacement of the spring-based model is much smaller than that of nonlinear models[54,55] (see the highlighted area in Fig. 5 in the work by Paneva *et al.*[55]), its linearity allows the unambiguous calculation of an activation for a given desired radiation force F_{rad} at minimal computational costs. If the focal point position x_f is always set sufficiently close to the actual position x of the object during its motion, we can use Hooke's law and derive a feasible x_f for a given F_{rad} under the knowledge of x and κ by simply transposing Eq. (2) to

$$x_f = \frac{F_{rad} + \kappa x}{\kappa}, \kappa \in \mathbb{R}^+. \tag{7}$$

Subsequently, an activation can be obtained by evaluating Eq. (5) with $r_0 = \begin{pmatrix} x_f & 0 & 0 \end{pmatrix}$. This algebraic relationship provides a simple, yet limited, solution in the unidimensional case that is only applicable in the proximity of the trapping point. Finally, this approach has a significant advantage over more sophisticated models,[55] where the general problem of ambiguity of the inverse projection $F_{rad}(r)$ persists due to the lack of differential flatness,[56] which inhibits the inversion of the dynamic model. To improve the contactless dynamic manipulation of objects, we use model-based trajectory planning. This control problem can be formulated as the determination of a feasible trajectory $u(t)$ for the focal point position $x_f(t)$ such that the position $x(t)$ of the sphere, taken as

measurable output $y(t)$ of the system, follows the given reference trajectory $w(t)$. The optimization problem can then be stated as minimizing the control error $e(t) = w(t) - y(t)$. Using the position $x(t)$ and the velocity $v(t)$ of the sphere as states $x_1(t)$ and $x_2(t)$ of the system, Eq. (2) can be rewritten as a system of two first-order differential equations. This results in the well-known representation of a non-autonomous linear system with a single input and a single output (SISO) in state space as

$$\begin{pmatrix} \dot{x}_1 \\ \dot{x}_2 \end{pmatrix} = \dot{x} = Ax + bu = \begin{pmatrix} 0 & 1 \\ -\dfrac{\kappa}{m} & -\dfrac{b}{m} \end{pmatrix} \begin{pmatrix} x_1 \\ x_2 \end{pmatrix} + \begin{pmatrix} 0 \\ \dfrac{\kappa}{m} \end{pmatrix} u, \tag{8}$$

$$y = c\,x = \begin{pmatrix} 1 & 0 \end{pmatrix} \begin{pmatrix} x_1 \\ x_2 \end{pmatrix},$$

where the time-dependency of the state $x(t)$, input $u(t)$, and output $y(t)$ were omitted due to brevity. Considering the constraints of the SISO system in Eq. (8), we first must ensure that Hooke's law is always valid, which results in a time-varying constraint of $u(t)$, which is given by

$$x_1(t) - d \le u(t) \le x_1(t) + d, \quad d = 1\text{mm}. \tag{9}$$

In addition, $u(t)$ is restricted by the serial interface between the PC and the FPGA (see Sec. II). For a baud rate of 250 kbit/s and a data package of 2580 bits (256 bytes for the phase angles, 2 bytes of commands, and one start and one stop bit for each transmitted byte) to be sent for an update of the activation of the phased array, $u(t)$ can only be changed every $T_c = 10.32$ ms and has to remain constant between two consecutive updates. This constraint can be interpreted as sampling $u(t)$ at a frequency of $f_c = 1/T_c$ and then reconstructing the resulting sequence $u[n]$ as a piecewise-constant signal with zero-order hold characteristics,

$$u(t) = u[n], n = \lfloor t/T_c \rfloor, n \in \mathbb{Z}. \tag{10}$$

To simplify matters, it is further assumed that the resulting radiation force is being immediately exerted on the object after an update of . Although the transient oscillations of the transducers during a phase change and the subsequent propagation of the emitted wave fronts are neglected by this assumption, the expected dead
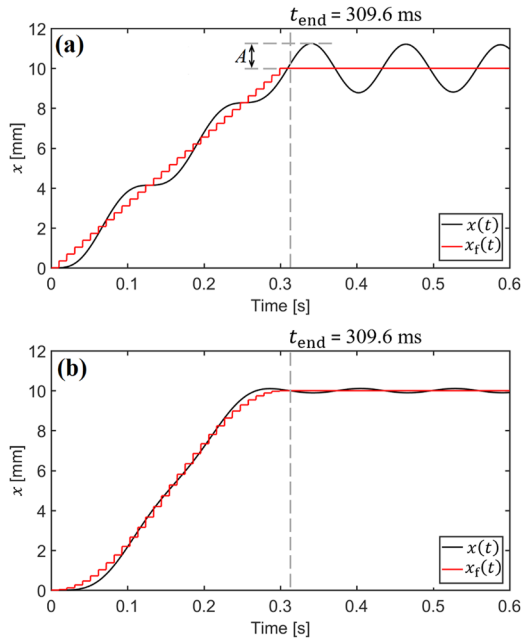
FIG. 4. Simulation of the sphere position over time $x(t)$ for two distinct manipulation strategies. (a) Linear motion. (b) Cosine motion. For both cases, the focal point position $x_f(t)$ was switched from $x_{start} = 0$ mm to $x_{end} = 10$ mm at a switching rate of $T_c = 10.32$ ms.
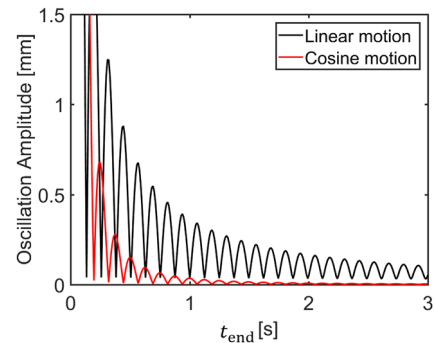
FIG. 5. Starting oscillation amplitude A after the focal point position $x_f(t)$ reaches the final position $x_{end} = 10$ mm as a function of total manipulation time t_{end}.

time T_d from these processes is very small in relation to T_c, resulting in a small error in each time interval $[nT_c, (n+1)T_c)$. Moreover, to the best of the authors' knowledge, it is currently unclear how the radiation force exerted on an object during a switch of the control variables of a phased array can be modeled with low computational costs and sufficient accuracy. Therefore, we encourage other authors to investigate this dynamic behavior to enhance the dynamics and accuracy of acoustic levitation systems. In addition, hardware resources limit the resolution of a transmitted activation to $\pi/16$ rad (see Sec. II). This causes a slight mismatch of the radiation force due to quantization errors of up to $\pi/32$ rad. As it can be seen from Fig. 2(b) in the supplementary material of the

FIG. 6. Comparison between the sphere position over time simulated by the dynamic model and that obtained experimentally for the linear and cosine motion strategies for different values of t_{end}. A video showing the sphere manipulation for a manipulation time of $t_{end} = 0.45$ s is available for both the linear and the cosine motion. Multimedia available online.

recent work by Andersson,[51] force magnitude errors of approximately up to 4% can be expected in our case for a sphere of a diameter of 2 mm when each phase angle is randomly perturbed by 5 . Although this error can be considered significant, we decided to neglect its influence here, mainly to avoid the formulation of complicated mixed-integer problems. After stating the SISO system and its constraints in Eqs. (8)–(10), we can formulate an optimal control problem[55] (OCP) for a given reference trajectory $w(t)$ with $t \in [0, T]$ and $T \gg T_c$ as

$$\min_{u(t)} \int_0^T \gamma(w(t) - y(t))^2 \mathrm{d}t, \quad (11)$$

$$\text{s.t.} \quad \dot{x}(t) = A x(t) + b u(t), \quad x(0) = x_0, \quad x(T) = x_T,$$
$$y(t) = c \, x(t),$$
$$u(t) = u[n], \quad n = \lfloor t/T_c \rfloor, \quad n \in \mathbb{Z},$$
$$|u(t) - x_1(t)| - d \le 0, \quad d = 1\text{mm},$$

where $\gamma \in \mathbb{R}^+$ is a positive hyperparameter. To solve the OCP, we decided to employ the model predictive control (MPC) toolbox in MATLAB. As MPC[57] is mainly an optimal control strategy for discrete systems, the continuous OCP was discretized by the toolbox using an implicit trapezoidal rule with a specified sample time of $T_s = T_c/100$. Furthermore, we chose T_c as the sample time of the controller and a zeroth-order interpolation scheme in each time interval $[nT_c, (n + 1)T_c]$ between two consecutive steps to reflect the restriction to $u(t)$ caused by the serial communication interface. Subsequently, after implementing Eq. (9) as a time-varying inequality constraint, we chose $\gamma = 500$ as well as $T_p = 10T_c$ as the prediction horizon and let the MPC toolbox determine a feasible $u(t)$ for the OCP.

VI. RESULTS AND DISCUSSION

A typical result calculated using the dynamic model given in Sec. III is presented in Fig. 4, which shows the simulated sphere position over time for the linear motion [Fig. 4(a)] and cosine motion [Fig. 4(b)] manipulation strategies. In both cases, the glass sphere is manipulated horizontally by changing the focal position from $x_f = 0$ mm to $x_f = 10$ mm in a total time of $t_{end} = 309.6$ ms in steps of $T_c = 10.32$ ms. Both $x_f(t)$ and the simulated sphere position over time $x(t)$ are shown in Figs. 4(a) and 4(b). For a very slow motion of $x_f(t)$, we could expect that the sphere would follow the position of the pressure node. Under this condition, a dynamic model would not be necessary since the sphere would present a quasi-static behavior. However, for a fast motion of the levitated sphere, such as the 309.6 ms manipulation time shown in Fig. 4, the sphere inertia becomes relevant, and the dynamic behavior should be considered to predict $x(t)$.

For the linear motion shown in Fig. 4(a), we can clearly see that $x(t)$ does not coincide with $x_f(t)$, but presents an oscillatory behavior with respect to the linear increase in $x_f(t)$. The frequency of this oscillatory behavior is ~8 Hz, which corresponds to the resonance frequency of 8.13 Hz along the x direction. For the cosine motion shown in Fig. 4(b), there is better agreement between $x_f(t)$ and $x(t)$ since the velocity of $x_f(t)$ does not have an abrupt increase at $t = 10.32$ ms, as it is the case for the linear motion. However, even for the cosine motion, the sphere presents a slight oscillatory behavior.

Figure 4 also shows that after the focal point position has reached $x_{end} = 10$ mm at $t_{end} = 309.6$ ms, the sphere presents a damped oscillatory motion. For the linear motion, the starting oscillation amplitude A after $t_{end} = 309.6$ ms is ~1.24 mm, whereas for the cosine motion, it yields $A = 0.11$ mm. Ideally, the oscillation amplitude after the sphere reaches x_{end} should be as small as possible, and for the particular result shown in Fig. 4, the cosine motion strategy outperforms the linear motion strategy.

To evaluate both strategies for different manipulation times, both manipulation strategies were simulated and the starting oscillation amplitude A after the focal point position reaches $x_f = 10$ mm was calculated as a function of manipulation time t_{end}. The comparison between both approaches is shown in Fig. 5. In general, the cosine motion strategy outperforms the linear motion strategy as the former presents smaller maximum oscillation amplitudes for similar times t_{end} and a faster decrease in the oscillation amplitudes with an increase in t_{end}. However, there are specific manipulation times where the linear motion strategy presents smaller oscillation amplitudes after the sphere reaches the final position $x = 10$ mm (e.g., for $t_{end} = 381.8$ ms, which corresponds to the third minimum of the black curve shown in Fig. 5). This usually occurs when the sphere reaches the final position $x = 10$ mm with low speeds. To understand this, we can observe the simulation result shown in Fig. 4(a). In this figure, the sphere reaches the position $x = 10$ mm with a velocity of 63 mm/s. Because of this high velocity, we have high oscillations after t_{end}. In the same figure, we could observe that if the manipulation was interrupted at $t = 258$ ms, we would have a low oscillation

FIG. 7. Focal positions over time $x_f(t)$ calculated by the MPC algorithm for a manipulation time $t_{end} = 0.45$ s: (a) linear motion; (b) cosine motion.

amplitude at the end since the sphere velocity at this time was small. Not surprisingly, t_{end} = 258 ms corresponds to one of the minima of the black curve shown in Fig. 5.

A neat explanation for the complicated relationship between t_{end} and the resulting oscillation amplitude can be found by examining the input signal $u(t)$. Due to the serial communication interface [see Eq. (10)], both manipulation strategies basically comprised a sequence of n impulses at intervals of T_c, which differ only in their amplitudes A_n at specific times t_n. Consequently, the response of the second-order system [see Eqs. (1) and (8)] to these impulses can be directly obtained by superimposing all impulses, similar to the derivation presented in Sec. IV in the work by Ahmad *et al.*[58] This relationship enables the prediction of the resulting oscillation amplitude at a specific point in time for a given input signal using an analytical equation without the need for a numerical simulation.

To verify the dynamic model for the linear and cosine motion manipulation strategies, the glass sphere was manipulated from x = 0 mm to x = 10 mm for different times t_{end}. The experimental position captured with the high-speed camera was compared with the position simulated by the dynamic model. The comparison between simulation and experimental sphere positions is presented in Fig. 6 (Multimedia available online). In general, there was good agreement between experimental and simulated results. The only exception occurred for t_{end} = 2.82 s, where A was significantly higher than predicted by the model. After t_{end} = 2.82 s, the experimental oscillation amplitude was $A \approx 0.25$ mm, whereas it yielded $A \approx 0.06$ mm for the simulated linear motion. This difference is attributed to regular oscillations that normally occur in acoustic levitation. The oscillation amplitude of $A \approx 0.25$ mm obtained in

this experiment is not too different from those shown in Fig. 2(a), where the focal point position is not moving. A similar behavior was also observed for the cosine motion strategy. After t_{end} = 2.82 s, A was also close to 0.25 mm, whereas the dynamic model predicted $A \leq 0.01$ mm. Again, this result is also explained by typical oscillations that normally occur in acoustic levitation. Despite this difference in the oscillation amplitude A, the proposed dynamic model usually provides reasonable results for predicting the sphere position over time.

According to the experimental and simulated results shown in Fig. 6 (Multimedia available online), the linear motion strategy is appropriate for slow manipulation speeds. For high manipulation speeds, oscillations during the sphere motion and after the focal point reaches the final position can be observed. This can be clearly seen for t_{end} = 0.45 s, where the sphere oscillates during its motion and presents a large oscillation amplitude after reaching its final position. In contrast to the linear motion strategy, the cosine motion strategy ensures a faster motion of the sphere with smaller oscillations during its manipulation.

In addition to the linear and cosine manipulation strategies, we also applied the MPC algorithm for calculating $x_f(t)$ to generate a linear motion and a cosine motion of the levitated sphere. The calculated values of $x_f(t)$ for the linear and cosine motion for t_{end} = 0.45 s are presented in Fig. 7.

The focal point positions obtained by the MPC algorithm (Fig. 7) were sent to the array to generate the linear and cosine motion. The comparison between the experimental and the simulated results is shown in Fig. 8 (Multimedia available online). In contrast to the linear motion strategy, shown in Fig. 6, in which a fast

FIG. 8. Comparison between simulated and experimental sphere positions over time for two different values of t_{end}. The MPC algorithm was used to obtain the focal position $x_f(t)$ to generate a linear and cosine motion of the levitating glass sphere. A video showing this experiment is available for both the linear and the cosine motion. Multimedia available online.

17 May 2024 14:15:04

linear motion results in oscillations of the sphere, the results shown in Fig. 8 indicate that the MPC algorithm allows us to generate a straight linear motion of the sphere with very small oscillations during its motion. Regarding the cosine motion generated by the MPC algorithm, the simulated and experimental results are not too different from those obtained with the standard cosine motion strategy (Fig. 6). However, the lower values for a_{max} and v_{max} shown in Fig. 8 compared to those shown in Fig. 6 indicate that the MPC algorithm is able to achieve an overall slightly smoother motion of the levitated sphere.

To ensure the feasibility of our proposed dynamic model, all the results of this paper were obtained for a unidimensional particle motion with a total displacement of 10 mm. In addition, the maximum manipulation speed was limited to moderate values such that the drag force acting on the sphere could be calculated by a simple linear drag model. Although the simplified dynamic model was able to predict the sphere position over time at sufficient accuracy, there are possible further improvements that could enhance the capability of the levitation system. For instance, the drag model could be improved to allow higher speeds of the levitated sphere. It could also be investigated how the trapping stiffness changes with the focal position, allowing the implementation of a better force model that is valid for larger manipulation distances. The force model could also be enhanced by considering a nonlinear trapping stiffness[54] instead of a simple model based on Hooke's law. In addition, the restrictions regarding the manipulation along the z direction, as described in Sec. II, could be resolved either by using a second phased array, replacing the reflector, or by employing nonlinear optimization techniques to obtain feasible activations for the phased array. Finally, our approach can be extended to allow the manipulation of liquid samples, either using a low driving voltage or taking into account the pressure-induced deformation of the levitated sample. To fully explore the capability of the presented methodology, future investigations are required.

VII. CONCLUSIONS

In this paper, we presented a simple dynamic model for calculating the position over time for a levitated sphere being moved in an acoustic levitator consisting of an array of transducers and an opposing reflector. In this model, the acoustic radiation force acting on the sphere is modeled by Hooke's law, and the drag force is assumed to be proportional to the velocity of the sphere. Using this model, we have calculated the sphere position over time for two manipulation strategies: a straight motion of constant velocity, called linear motion strategy, and a straight motion where the sphere is subjected to a cosine function acceleration (cosine motion). In addition, we have applied an MPC algorithm for calculating the focal point positions to generate a linear and a cosine motion of the sphere. The simulated results were verified experimentally by tracking the position of the sphere with a high-speed camera. Despite the simplicity of the proposed model, the comparison between experiment and simulation presents good agreement, indicating that the dynamic model can be used for predicting the dynamic behavior of the acoustically manipulated sphere. Moreover, a comparison between the linear and the cosine manipulation strategy suggests that the cosine manipulation strategy outperforms the linear strategy, allowing faster manipulation speeds with reduced oscillations.

By applying MPC to the path-following problem in Eq. (11), it is possible to take additional time-variant constraints of the states, that is, the manipulated variables of a system, into account, which is a huge advantage compared to classical input-shaping techniques, such as those presented in the work by Ahmad et al.[58] The versatility of MPC further allows the realization of additional trajectories for various t_{end} values in a model-based feedforward control to move the levitated object smoothly to its target position along a desired path. This smooth motion cannot always be achieved using predefined analytical strategies, as can be seen when comparing Figs. 6 and 8. Therefore, the use of MPC considerably facilitates trajectory planning and eliminates the burden to carry out several numerical simulations to manually test different t_{end} values for a desired trajectory in advance. Although the presented dynamic model can predict the dynamic behavior of the acoustically manipulated sphere with sufficient accuracy in our application, there are two points that can be improved to increase its accuracy and generalizability. First, it might be worthwhile to model the transient behavior of the transducers during phase changes as well as the subsequent time delays caused by the propagation of the emitted wave fronts to the levitated object. With this knowledge, it will be possible to approximate the acoustic radiation force exerted on the object during a change in the control variables, which is crucial for excellent control performance. Since the expected dead time T_d from these processes is very small in relation to the switching time T_c, it certainly can be supposed that the resulting radiation force error for a single change is also small when an instantaneous change in the radiation force is assumed (see Sec. V). However, since an input $u(t)$ is optimized according to a dynamic model for a given reference trajectory in trajectory planning, it cannot be ruled out for the experimental tests that such a small error for a single change in $u(t)$ will be amplified over a certain input sequence that is applied to the system. This could also explain the relatively large deviations between simulation and experiment that have occurred in our tests only for a few control sequences, for example, in Fig. 6, for t_{end} = 2.82 s during the time interval $t \in [0, 2.82\ s]$. Second, it is necessary to find a more generalizable approach for the inversion of the dynamic model to enable the model-based trajectory planning of a three-dimensional motion of a levitated particle along arbitrary paths rather than restricting its movement to a unidimensional motion along the main axis of an acoustic trap.

Finally, the presented method of iterative phase-refocusing together with Hooke's law [see Eqs. (5) and (7)] is well-suited for future usage in a model-based closed-loop control since it has minimal computational costs due to the algebraic relationship between F_{rad} and   . Such a closed-loop control is a mandatory requirement to use acoustic levitation systems not only in academic research, as it is the case today, but also in future industrial applications, enabling the precise placement and fast manipulation of levitated objects.

SUPPLEMENTARY MATERIAL

See the supplementary material for more details on approximating the acoustic radiation force by Hooke's law and for a numerical model for calculating the acoustic radiation force that acts on a small rigid sphere.

<div style="writing-mode: vertical">17 May 2024 14:15:04</div>

AUTHOR DECLARATIONS

Conflict of Interest

The authors have no conflicts to disclose.

Author Contributions

Marco A. B. Andrade: Conceptualization (equal); Funding acquisition (equal); Methodology (equal); Writing – original draft (equal). **Sebastian Zehnter**: Methodology (equal); Writing – original draft (equal); Writing – review & editing (equal). **Felix Funke**: Methodology (equal); Writing – review & editing (equal). **Christoph Ament**: Funding acquisition (equal); Supervision (lead); Writing – review & editing (equal).

DATA AVAILABILITY

The data that support the findings of this study are available within the article and from the corresponding author upon reasonable request.

REFERENCES

[1] M. A. B. Andrade, A. Marzo, and J. C. Adamowski, Appl. Phys. Lett. **116**, 250501 (2020).

[2] H. Bruus, Lab Chip **12**, 1014 (2012).

[3] A. L. Yarin, M. Pfaffenlehner, and C. Tropea, J. Fluid Mech. **356**, 65 (1998).

[4] D. Zang, Y. Yu, Z. Chen, X. Li, H. Wu, and X. Geng, Adv. Colloid Interface Sci. **243**, 77 (2017).

[5] W. J. Xie and B. Wei, Phys. Rev. E **70**, 046611 (2004).

[6] M. A. B. Andrade, A. L. Bernassau, and J. C. Adamowski, Appl. Phys. Lett. **109**, 044101 (2016).

[7] S. Santesson and S. Nilsson, Anal. Bioanal. Chem. **378**, 1704 (2004).

[8] A. Scheeline and R. L. Behrens, Biophys. Chem. **165-166**, 1 (2012).

[9] C. J. Benmore and J. K. R. Weber, Phys. Rev. X **1**, 011004 (2011).

[10] C. J. Benmore, J. K. R. Weber, A. N. Tailor, B. R. Cherry, J. L. Yarger, Q. Mou, W. Weber, J. Neuefeind, and S. R. Byrn, J. Pharm. Sci. **102**, 1290 (2013).

[11] V. Vandaele, P. Lambert, and A. Delchambre, Precis. Eng. **29**, 491 (2005).

[12] S. Ueha, Y. Hashimoto, and Y. Koike, Ultrasonics **38**, 26 (2000).

[13] M. Takasaki, D. Terada, Y. Kato, Y. Ishino, and T. Mizuno, Phys. Proc. **3**, 1059 (2010).

[14] M. A. B. Andrade, T. S. Ramos, J. C. Adamowski, and A. Marzo, Appl. Phys. Lett. **116**, 054104 (2020).

[15] A. Marzo, M. Caleap, and B. W. Drinkwater, Phys. Rev. Lett. **120**, 044301 (2018).

[16] W. J. Xie and B. Wei, Phys. Rev. E **66**, 026605 (2002).

[17] W. J. Xie, C. D. Cao, Y. J. Lü, and B. Wei, Phys. Rev. Lett. **89**, 104304 (2002).

[18] D. Foresti, M. Nabavi, M. Klingauf, A. Ferrari, and D. Poulikakos, Proc. Natl. Acad. Sci. U. S. A. **110**, 12549 (2013).

[19] T. Kozuka, K. Yasui, T. Tuziuti, A. Towata, and Y. Iida, Jpn. J. Appl. Phys. **46**, 4948 (2007).

[20] Y. Ochiai, T. Hoshi, and J. Rekimoto, PLoS One **9**, e97590 (2014).

[21] J. K. R. Weber, C. A. Rey, J. Neuefeind, and C. J. Benmore, Rev. Sci. Instrum. **80**, 083904 (2009).

[22] E. Trinh, J. Robey, N. Jacobi, and T. Wang, J. Acoust. Soc. Am. **79**, 604 (1986).

[23] D. Koyama and K. Nakamura, IEEE Trans. Ultrason., Ferroelectr. Freq. Control **57**, 1152 (2010).

[24] C. R. Field and A. Scheeline, Rev. Sci. Instrum. **78**, 125102 (2007).

[25] M. A. B. Andrade, F. C. Buiochi, and J. Adamowski, IEEE Trans. Ultrason., Ferroelectr. Freq. Control **57**, 469 (2010).

[26] T. Hoshi, Y. Ochiai, and J. Rekimoto, Jpn. J. Appl. Phys. **53**, 07KE07 (2014).

[27] A. Watanabe, K. Hasegawa, and Y. Abe, Sci. Rep. **8**, 10221 (2018).

[28] M. A. B. Andrade, T. S. A. Camargo, and A. Marzo, Rev. Sci. Instrum. **89**, 125105 (2018).

[29] A. Marzo, S. A. Seah, B. W. Drinkwater, D. R. Sahoo, B. Long, and S. Subramanian, Nat. Commun. **6**, 8661 (2015).

[30] A. Marzo and B. W. Drinkwater, Proc. Natl. Acad. Sci. U. S. A. **116**, 84 (2019).

[31] I. Ezcurdia, R. Morales, M. A. B. Andrade, and A. Marzo, in *Conference Proceedings on Special Interest Group on Computer Graphics and Interactive Techniques* (ACM, New York, 2022), pp. 1–9.

[32] R. H. Morris, E. R. Dye, P. Docker, and M. I. Newton, Phys. Fluids **31**, 101301 (2019).

[33] S. Zehnter, M. A. B. Andrade, and C. Ament, J. Appl. Phys. **129**, 134901 (2021).

[34] R. Hirayama, D. Martinez Plasencia, N. Masuda, and S. Subramanian, Nature **575**, 320 (2019).

[35] R. Hirayama, G. Christopoulos, D. Martinez Plasencia, and S. Subramanian, Sci. Adv. **8**, eabn7614 (2022).

[36] G. Memoli, M. Caleap, M. Asakawa, D. R. Sahoo, B. W. Drinkwater, and S. Subramanian, Nat. Commun. **8**, 14608 (2017).

[37] M. A. B. Andrade, N. Pérez, and J. C. Adamowski, J. Acous. Soc. Am. **136**, 1518 (2014).

[38] K. Hasegawa and K. Kono, AIP Adv. **9**, 035313 (2019).

[39] R. Morales, I. Ezcurdia, J. Irisarri, M. A. B. Andrade, and A. Marzo, Appl. Sci. **11**, 2981 (2021).

[40] A. Marzo, T. Corkett, and B. W. Drinkwater, IEEE Trans. Ultrason. Ferroelectrics Freq. Control **65**, 102 (2018).

[41] M. Barmatz and P. Collas, J. Acoust. Soc. Am. **77**, 928 (1985).

[42] M. A. B. Andrade, N. Pérez, and J. C. Adamowski, Braz. J. Phys. **48**, 190 (2018).

[43] E. H. Trinh and J. L. Robey, Phys. Fluids **6**, 3567 (1994).

[44] K. Hasegawa, Y. Abe, A. Kaneko, Y. Yamamoto, and K. Aoki, Microgravity Sci. Technol. **21**, S9 (2009).

[45] K. Kobayashi, A. Goda, K. Hasegawa, and Y. Abe, Phys. Fluids **30**, 082105 (2018).

[46] C. Andersson and J. Ahrens, in *Sensor Array and Multichannel Signal Processing Workshop* (IEEE, 2018), pp. 622–626.

[47] T. Puranen, E. Haggstrom, P. Helander, A. Merilainen, G. Maconi, A. Penttila, M. Gritsevich, I. Kassamakov, A. Salmi, and K. Muinonen, *2019 IEEE International Ultrasonics Symposium* (IEEE, 2019), pp. 916–919.

[48] L. P. Gor'kov, Sov. Phys. Dokl. **6**, 773 (1962).

[49] M. A. Abdelaziz and D. G. Grier, Phys. Rev. Res. **2**, 013172 (2020).

[50] S. Inoue, S. Mogami, T. Ichiyama, A. Noda, Y. Makino, and H. Shinoda, J. Acous. Soc. Am. **145**, 328 (2019).

[51] C. Andersson, J. Acoust. Soc. Am. **151**, 2999 (2022).

[52] M. Bachynskyi, V. Paneva, and J. Müller, in *Proceedings of the 2018 ACM International Conference on Interactive Surfaces and Spaces* (ACM, New York, 2018), pp. 253–262.

[53] L. Jiang, Y. Wang, S. Fan, X. Yu, and X. Li, Mechatronics **92**, 102984 (2023).

17 May 2024 14:15:04

[54] T. Fushimi, T. L. Hill, A. Marzo, and B. W. Drinkwater, Appl. Phys. Lett. **113**, 034102 (2018).

[55] V. Paneva, A. Fleig, D. M. Plasencia, T. Faulwasser, and J. Müller, ACM Trans. Graphics **41**, 1 (2022).

[56] M. Fliess, J. Lévine, P. Martin, and P. Rouchon, Int. J. Control **61**, 1327 (1995).

[57] L. Grüne and J. Pannek, *Nonlinear Model Predictive Control* (Springer International Publishing, Cham, 2017).

[58] M. A. Ahmad, R. M. T. R. Ismail, and M. S. Ramli, in *2009 International Conference on Mechatronics and Automation* (IEEE, 2009), pp. 2876–2881.

17 May 2024 14:15:04